Nonlinear vibrations of a piecewise-linear quarter-car truck model by incremental harmonic balance method

Sheng Wang · Lin Hua · Can Yang · Yong'ou Zhang · Xiaodong Tan

Abstract A two-degree-of-freedom (2DOF) quarter-car model with a piecewise leaf spring for the rear suspension of a truck is presented. A leaf spring, which contains a main leaf and an auxiliary leaf, can be regarded as a model with piecewise-linear stiffness and damping, and the model is built with two load states according to whether the auxiliary leaf spring is at work at the static equilibrium. The incremental harmonic balance method is used to obtain the nonlinear dynamics of the presented quarter-car truck model. The accuracy of this method is verified by comparing the nonlinear responses, including the sub-harmonic resonance, with the Runge–Kutta method. Afterward, the effects of the auxiliary leaf spring's stiffness, the sprung mass ratio and the main leaf spring's damping on the dynamic responses of the system are investigated. It is found that the piecewise-linear system shares similar dynamic characteristics with a Duffing oscillator, and the proper design of the auxiliary leaf spring can contribute to the reduction in the fundamental resonance amplitudes of the system. The frequency response curve shows 'snap-back' features in the sub-harmonic resonance under a certain sprung mass and the leaf spring's damping, which is due to the coupled nonlinearities of both DOFs. In addition, the increase of the main leaf spring's damping can shrink or even eliminate the sub-harmonic or chaos resonances.

S. Wang · L. Hua (✉) · C. Yang · X. Tan
School of Automotive Engineering, Wuhan University of Technology, Wuhan 430070, China
e-mail: hualin@whut.edu.cn

S. Wang
e-mail: wangs@whut.edu.cn

C. Yang
e-mail: yangcan@whut.edu.cn

X. Tan
e-mail: tandengken@163.com

L. Hua
Hubei Key Laboratory of Advanced Technology of Automotive Parts, Wuhan 430070, China

L. Hua
Hubei Collaborative Innovation Center for Automotive Components Technology, Wuhan 430070, China

Y. Zhang
School of Transportation, Wuhan University of Technology, Wuhan 430070, China
e-mail: zhangyo@whut.edu.cn

1 Introduction

Nowadays, with the development of lightweight technology on vehicles, there are many applications of leaf springs with variable stiffness on the design of suspensions. Compared with traditional leaf springs, these leaf springs have the advantages of lightness of weight, comfortability in riding, enhancement of carrying capacity, etc. In the vehicle design of a leaf spring suspension, the suspension that contains a main leaf

spring and an auxiliary leaf spring has often been used, especially in trucks that carry a wide variety of loads. Usually, the design on the lightness of weight would cause a low performance on vibration; thus, the dynamics of the suspension are an essential part of suspension design and optimization [1]. Many scholars have proposed the quarter-car model to analyze the dynamics of the suspension system [2–7], which can be adopted to evaluate a piecewise-linear leaf spring suspension [8–12]. The perturbation methods seem to be a universal way to predict the responses of this type of vehicle suspension system. Zhong et al. [8] proposed a 2-DOF piecewise-linear leaf spring suspension model, and the average method was used to investigate the nonlinear dynamics of the system, and the transition sets; 40 groups of bifurcation curves were found with various system parameters. Li et al. [9] used the average method to study the effects of a mass variation of the dynamic response of the SDOF piecewise-linear suspension system. Silveira et al. [10] discussed the 2-DOF quarter-car model with piecewise-linear damping under harmonic excitation, and the results showed that the piecewise damping ratio directly influenced the maximum displacement, speed and acceleration of the sprung mass. Deshpande et al. [11] studied a more general piecewise-linear vibration isolation system with secondary suspension, the characteristic of the jump-free zones was investigated and a boundary surface between no-jump (unique response) and jump areas was established.

However, the perturbation methods are only suitable for weakly nonlinear problems. Bajkowski et al. [12] showed that amplitude–frequency response curves from the averaging method and the numerical method became different when there were strong nonlinearities in the system. Some piecewise-linear characteristics, such as super-harmonic and sub-harmonic resonance are difficult to obtain with these methods. The IHBM that was proposed by Cheung [13] is an effective method for solving both weakly and strongly nonlinear problems under periodic excitations [14–16]. Zhou [2] studied the vehicle suspension system with nonlinear stiffness and damping through IHBM and the numerical method, and the results of these methods showed good agreement. Regarding the piecewise-linear problems, IHBM also provided a systematic procedure by introducing the step functions [18,19]. Various piecewise-linear system dynamics have been investigated with this method [17,20–28]. The accuracy of the IHBM results of piecewise-linear systems has also been con-

sistent with the accuracy of the numerical method, including super-harmonic and sub-harmonic resonance [24]. In addition, to track the unstable response or sub-harmonic resonance, many continuous methods have been used to acquire the frequency response curves including the incremental arc-length method combined with a cubic extrapolation technique [13]; Broyden's method [16]; arc-length method [17,24,27], etc.

By using IHBM, the super-harmonic and sub-harmonic resonance of piecewise-linear systems can also be predicted. Wong et al. [18] showed that the bifurcation of the $1/m$ sub-harmonic resonances can be found on the right side of the fundamental resonance's peak and m super-harmonic resonances on the left side in the SDOF piecewise-linear system by using IHBM. Lau et al. [19] considered a SDOF system with symmetric piecewise stiffness, it was found that the sub-harmonic response shrinks into complicated closed curves in the presence of damping. Kim et al. [24] studied a reduced order torsional system with symmetric piecewise stiffness using IHBM with adaptive arc-length continuation, and the results showed that the appearance of sub-harmonic resonance depends on the frequency separation between the primary harmonic of the compliant side and the mean operating point crossover position to the stiffness transitions. Duan et al. [25] used multi-term IHBM to analyze a family of isolated sub-harmonic branches in the nonlinear frequency response of piecewise-linear systems and concluded that the relationship between the linear mean operating and transition points rather than asymmetric piecewise stiffness appeared to be the key factor that generated the isolated branches.

Although many articles have been devoted to SDOF piecewise systems that consider sub/super-harmonic resonances, the literature has reported few studies on multiple DOF piecewise systems, especially when the added DOFs could affect these resonances of the system. In the present paper, considering the piecewise-linear stiffness and damping of the suspension, the nonlinear responses, including the sub-harmonic response, of a 2-DOF piecewise-linear quarter-car model are studied with IHBM. Because of the different types of local dynamic behaviors, the piecewise-linear suspension model is built by two load states according to whether the auxiliary leaf spring is at work at the static equilibrium. This paper is organized as follows. Section 2 establishes a 2-DOF quarter-car model with a piecewise-linear leaf spring for the rear suspension of
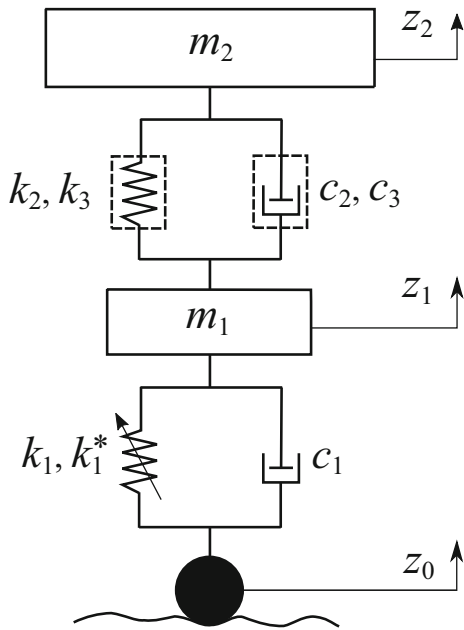
Fig. 1 Schematic model of a piecewise-linear quarter-car model

a truck. In Sect. 3, IHBM is derived to obtain the nonlinear motions of the present model subject to the external road profile. The results of IHBM are validated by the Runge–Kutta method, and the effect of some key system parameters on the dynamic response of the present models is studied in Sect. 4. Finally, Sect. 5 draws some conclusions from the present work.

2 The quarter-car system

The dynamic system of a 2-DOF quarter-car truck model with a piecewise-linear leaf spring is shown in Fig. 1. When the sprung load on the leaf spring is small, only the main leaf spring works. The distance between the main leaf spring and the auxiliary leaf spring decreases as the load increases. On the critical sprung load where the distance becomes zero, the auxiliary leaf spring exactly begins to work. As the sprung load continues to increase, both leaf springs work. In this paper, the variable z_1 represents the unsprung mass vertical displacement, z_2 is the sprung mass vertical displacement, and z_0 is the road profile. The road profile is expressed by

$$z_0 = r \sin(\omega t) \tag{1}$$

where r and ω are the amplitude and frequency, respectively, of the harmonic road profile.

Other parameters that are shown in Fig. 1 are defined as follows. m_1 and m_2 are the unsprung mass and the sprung mass, respectively, of the truck. k_1 and k_1^* are the nonlinear coefficients of the tire stiffness, and the tire stiffness can be approximately regarded as a quadratic curve-fitting model. Equation (2) gives the curve-fitting form:

$$g_N(x) = k_1 x + k_1^* x^2 \tag{2}$$

where c_1 is the tire damping, k_2 and k_3 are the stiffness of the main and auxiliary leaf springs, respectively, c_2 and c_3 are the damping of the main and auxiliary leaf springs, respectively, e represents the distance between the main leaf spring and the auxiliary leaf spring when the two leaf springs are at the no-load state, and d_1 and d_2 are the critical distances, namely, the distances between the position where the sprung mass is loaded at the state of static equilibrium and the critical position where the auxiliary leaf spring exactly does not work. d_1 and d_2 can be defined as

$$d_1 = e - \frac{m_2 g}{k_2}, d_2 = \frac{m_2 g - k_2 e}{k_2 + k_3} \tag{3}$$

To investigate the nonlinear motions of the 2-DOF system, the relative displacements are used as follows:

$$z_{21} = z_2 - z_1$$
$$z_{10} = z_1 - z_0 \tag{4}$$

In this work, the origin coordinates are set to the static balance position to ignore the gravity of the system. As seen in Fig. 2, the static balance position of system is divided into two states because of the variation of the sprung mass: the light load state and the heavy load state. Additionally, the two different load states are also relevant to the local dynamic behaviors of the primary resonances, which are studied in Sect. 4.2. The critical sprung mass can be obtained with Eq. (5).
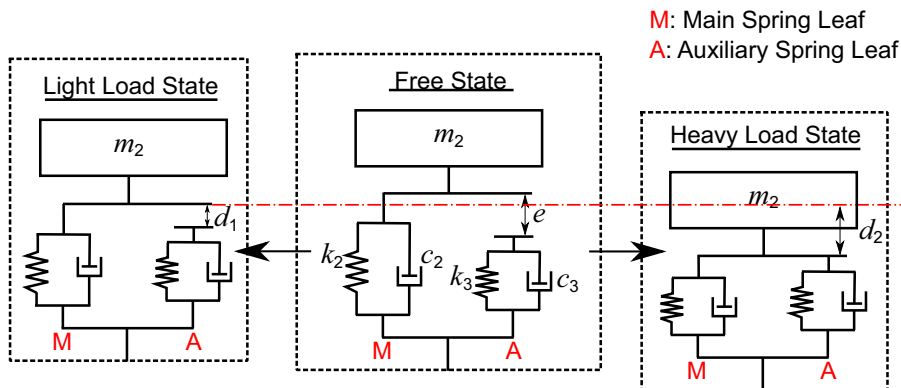
$$m_{2cr} = \frac{k_2 e}{g} \tag{5}$$

By applying the Newtonian law, the dynamic equations of the light load state and the heavy load state can be obtained.

For the light load state,

$$m_2(\ddot{z}_0 + \ddot{z}_{10} + \ddot{z}_{21}) + c_2 \dot{z}_{21} + k_2 z_{21}$$
$$+ f_1(z_{21}, \dot{z}_{21}) = 0$$

Fig. 2 Load state definitions of the piecewise-linear spring leaf

M: Main Spring Leaf
A: Auxiliary Spring Leaf

$$m_1(\ddot{z}_0 + \ddot{z}_{10}) - c_2\dot{z}_{21}$$
$$- k_2 z_{21} - f_1(z_{21}, \dot{z}_{21}) + c_1\dot{z}_{10} + g_N(z_{10}) = 0$$
$$(6)$$

For the heavy load state,

$$m_2(\ddot{z}_0 + \ddot{z}_{10} + \ddot{z}_{21}) + (c_2 + c_3)\dot{z}_{21}$$
$$+ (k_2 + k_3)z_{21} + f_2(z_{21}, \dot{z}_{21}) = 0$$
$$m_1(\ddot{z}_0 + \ddot{z}_{10}) - (c_2 + c_3)\dot{z}_{21} - (k_2 + k_3)z_{21}$$
$$- f_2(z_{21}, \dot{z}_{21}) + c_1\dot{z}_{10} + g_N(z_{10}) = 0 \qquad (7)$$

where the overhead dot represents the differentiation with respect to time t. $f_1(z_{21}, \dot{z}_{21})$ and $f_2(z_{21}, \dot{z}_{21})$ are the piecewise-linear functions that represent the auxiliary leaf spring forces:

$$f_1(z_{21}, \dot{z}_{21}) = \begin{cases} c_3\dot{z}_{21} + k_3(z_{21} + d_1) & z_{21} < -d_1 \\ 0, & z_{21} \geq -d_1 \end{cases}$$
$$(8)$$

$$f_2(z_{21}, \dot{z}_{21}) = \begin{cases} 0, & z_{21} < d_2 \\ -c_3\dot{z}_{21} - k_3(z_{21} - d_2), & z_{21} \geq d_2 \end{cases}$$
$$(9)$$

To simplify the above equations, the following dimensionless quantities are introduced:

$$\omega_1 = \sqrt{\frac{k_1}{m_1}}, \xi = \frac{c_1}{2\sqrt{m_1 k_1}}, t' = \omega_1 t, v_2$$
$$= \frac{k_2}{k_1}, v_3 = \frac{k_3}{k_1}, \eta_2 = \frac{c_2}{c_1}, \eta_3 = \frac{c_3}{c_1},$$
$$x_1 = \frac{z_{10}}{r}, x_2 = \frac{z_{21}}{r}, D = \frac{e}{r}, \alpha = \frac{k_1^*}{k_1}r, v$$
$$= \frac{m_1 g}{k_1 r}, \mu = \frac{m_2}{m_1}, \Omega = \frac{\omega}{\omega_1},$$
$$\mu_{cr} = \frac{k_2 e}{m_1 g}, \Delta_1 = -\frac{d_1}{r}, \Delta_2 = \frac{d_2}{r} \qquad (10)$$

For the piecewise-linear equations, the step function is used to make the derivation simpler [18]:

$$h_{(x_2 - \Delta_1)} = \begin{cases} 1 & x_2 < \Delta_1 \\ 0 & x_2 \geq \Delta_1 \end{cases} \qquad (11)$$

$$h_{(x_2 - \Delta_2)} = \begin{cases} 0 & x_2 < \Delta_2 \\ -1 & x_2 \geq \Delta_2 \end{cases} \qquad (12)$$

Thus, the step functions have a unified form for both states:

$$h_{(x_2 - \Delta)} = \begin{cases} h_{(x_2 - \Delta_1)}\mu < \mu_{cr}, & \Delta = \Delta_1 \\ h_{(x_2 - \Delta_2)}\mu \geq \mu_{cr}, & \Delta = \Delta_2 \end{cases} \qquad (13)$$

Letting

$$c = \begin{cases} \eta_2, & \mu < \mu_{cr} \\ \eta_2 + \eta_3, & \mu \geq \mu_{cr} \end{cases} \qquad (14)$$

$$k = \begin{cases} v_2, & \mu < \mu_{cr} \\ v_2 + v_3, & \mu \geq \mu_{cr} \end{cases} \qquad (15)$$

$$G = h_{(x_2 - \Delta)}(v_3(x_2 - \Delta) + 2\xi\eta_3\dot{x}_2) \qquad (16)$$

$$\mathbf{q} = \begin{bmatrix} x_1 & x_2 \end{bmatrix}^T = \begin{bmatrix} q_1 & q_2 \end{bmatrix}^T \qquad (17)$$

$$\bar{\mathbf{M}} = \begin{bmatrix} \mu & \mu \\ 1 & 0 \end{bmatrix} \qquad (18)$$

$$\bar{\mathbf{C}}_L = \begin{bmatrix} 0 & 2\xi c \\ 2\xi & -2\xi c \end{bmatrix} \qquad (19)$$

$$\bar{\mathbf{K}}_L = \begin{bmatrix} 0 & k \\ 1 & -k \end{bmatrix} \qquad (20)$$

$$\bar{\mathbf{G}}_{NL} = \begin{bmatrix} G \\ -G + \alpha x_1^2 \end{bmatrix} \qquad (21)$$

$$\bar{\mathbf{F}} = \begin{bmatrix} \mu \\ 1 \end{bmatrix} \qquad (22)$$

By substituting Eqs. (13)–(22) into Eqs. (6)–(9), the dynamic equations can be rewritten with the matrix form:

$$\bar{\mathbf{M}}\ddot{\mathbf{q}} + \bar{\mathbf{C}}_L\dot{\mathbf{q}} + \bar{\mathbf{K}}_L\mathbf{q} + \bar{\mathbf{G}}_{NL} = \Omega^2 \sin(\Omega t')\bar{\mathbf{F}} \qquad (23)$$

where the overhead dot represents the differentiation with respect to time t'.

3 IHBM for piecewise-linear system

3.1 IHBM scheme

In this section, the IHBM procedures are adopted to solve Eq. (23). Letting $\tau = \Omega t'$, Eq. (23) can be rewritten as

$$\Omega^2 \bar{\mathbf{M}}\ddot{\mathbf{q}} + \Omega \bar{\mathbf{C}}_L \dot{\mathbf{q}} + \bar{\mathbf{K}}_L \mathbf{q} + \bar{\mathbf{G}}_{NL} - \Omega^2 \sin(\tau)\bar{\mathbf{F}} = \mathbf{0} \tag{24}$$

where the overhead dot represents the differentiation with respect to time τ, and Ω is the non-dimensional excitation frequency of relevance. Let $\mathbf{q}_{i0}$ and Ω_0 denote the state of vibration in hand, and the neighboring state can be expressed by adding the corresponding increments to them [13]:

$$\mathbf{q} = \mathbf{q}_0 + \Delta\mathbf{q}, \Omega = \Omega_0 + \Delta\Omega \tag{25}$$

where $\mathbf{q} = [\mathbf{q}_{10}, \mathbf{q}_{20}]^T$ and $\Delta\mathbf{q} = [\Delta\mathbf{q}_1, \Delta\mathbf{q}_2]^T$.

By substituting Eq. (25) into Eq. (24), the following incremental equation can be obtained by neglecting the high-order incremental terms:

$$\Omega_0^2 \bar{\mathbf{M}}\Delta\ddot{\mathbf{q}} + \Omega_0(\bar{\mathbf{C}}_L + \bar{\mathbf{C}}_{NL})\Delta\dot{\mathbf{q}}$$
$$+ (\bar{\mathbf{K}}_L + \bar{\mathbf{K}}_{NL})\Delta\mathbf{q} = \bar{\mathbf{R}} + \bar{\mathbf{R}}_{mc}\Delta\Omega \tag{26}$$

Here, the unknown matrices can be expressed as follows:

$$\bar{\mathbf{C}}_{NL} = \begin{bmatrix} 0 & 2h_{(q_{20}-\Delta)}\xi c \\ 0 & -2h_{(q_{20}-\Delta)}\xi c \end{bmatrix} \tag{27}$$

$$\bar{\mathbf{K}}_{NL} = \begin{bmatrix} 0 & h_{(q_{20}-\Delta)}k \\ 2\alpha q_{10} & -h_{(q_{20}-\Delta)}k \end{bmatrix} \tag{28}$$

$$\bar{\mathbf{E}}_N = \begin{bmatrix} h_{(q_{20}-\Delta)}k(q_{20} - \Delta) \\ -h_{(q_{20}-\Delta)}k(q_{20} - \Delta) + \alpha q_{10}^2 \end{bmatrix} \tag{29}$$

$$\bar{\mathbf{R}} = -(\Omega_0^2 \bar{\mathbf{M}}\ddot{\mathbf{q}}_0 + \Omega_0(\bar{\mathbf{C}}_L + \bar{\mathbf{C}}_{NL})\dot{\mathbf{q}}_0 + \bar{\mathbf{K}}_L\mathbf{q}_0)$$
$$- \bar{\mathbf{E}}_N + \Omega_0^2 \sin(\tau)\bar{\mathbf{F}} \tag{30}$$

$$\bar{\mathbf{R}}_{mc} = -2\Omega_0\bar{\mathbf{M}}\ddot{\mathbf{q}}_0 - (\bar{\mathbf{C}}_L + \bar{\mathbf{C}}_{NL})\dot{\mathbf{q}}_0 + 2\Omega_0 \sin(\tau)\bar{\mathbf{F}} \tag{31}$$

Then, the harmonic balance procedure is adopted. Given the periodic solution with a truncated finite Fourier series,

$$q_{j0}(\tau) = \frac{1}{2}a_{j0} + \sum_{i=1}^{N}\left(a_{ji}\cos\frac{i\tau}{m} + b_{ji}\sin\frac{i\tau}{m}\right)$$
$$= \mathbf{C}_s\mathbf{A}_j \tag{32}$$

$$\Delta q_j(\tau) = \frac{1}{2}\Delta a_{j0} + \sum_{i=1}^{N}\left(\Delta a_{ji}\cos\frac{i\tau}{m} + \Delta b_{ji}\sin\frac{i\tau}{m}\right)$$
$$= \mathbf{C}_s\Delta\mathbf{A}_j \tag{33}$$

where N is the number of the harmonic terms used in the solution, and m is the order of the sub-harmonic solution. Other parameters are expressed below:

$$\mathbf{C}_s = \left[\frac{1}{2}, \cos\frac{\tau}{m}, \ldots, \cos\frac{N\tau}{m}, \sin\frac{\tau}{m}, \ldots, \sin\frac{N\tau}{m}\right] \tag{34}$$

$$\mathbf{S} = \text{diag}\left[\mathbf{C}_s, \mathbf{C}_s\right] \tag{35}$$

$$\mathbf{A}_j = \left[a_{j0}, a_{j1}, \ldots, a_{jN}, b_{j1}, \ldots, b_{jN}\right]^T, j = 1, 2 \tag{36}$$

$$\Delta\mathbf{A}_j = \left[\Delta a_{j0}, \Delta a_{j1}, \ldots, \Delta a_{jN}, \Delta b_{j1}, \ldots, \Delta b_{jN}\right]^T,$$
$$j = 1, 2 \tag{37}$$

$$\mathbf{A} = \left[\mathbf{A}_1, \mathbf{A}_2\right]^T, \Delta\mathbf{A} = \left[\Delta\mathbf{A}_1, \Delta\mathbf{A}_2\right]^T \tag{38}$$

According to the above equations, the vectors of the non-dimensional displacement unknowns and their increments can be expressed as

$$\mathbf{q}_0 = \mathbf{S}\mathbf{A}, \Delta\mathbf{q} = \mathbf{S}\Delta\mathbf{A} \tag{39}$$

The positive integer m and N introduced in Eqs. (32) and (33) should be chosen according to the number of period-m bifurcations that the system has undergone [15]. $m = 1$ and $N = N_m$ for the period-1 solution, and $m = p$ and $N = pN_m$ for the period-p solution (where $p = 2, 3, \ldots$). N_m is determined in terms of the required computing accuracy, which is studied in Sect. 4.1.

The Galerkin procedure is performed as follows:

$$\int_0^{2m\pi}\left[\Omega_0^2\bar{\mathbf{M}}\Delta\ddot{\mathbf{q}} + \Omega_0(\bar{\mathbf{C}}_L + \bar{\mathbf{C}}_{NL})\Delta\dot{\mathbf{q}} + (\bar{\mathbf{K}}_L\right.$$
$$\left.+ \bar{\mathbf{K}}_{NL})\Delta\mathbf{q}\right]\delta(\Delta\mathbf{q})\,d\tau$$
$$= \int_0^{2m\pi}\left(\bar{\mathbf{R}} + \bar{\mathbf{R}}_{mc}\Delta\Omega\right)\delta(\Delta\mathbf{q})d\tau \tag{40}$$

By substituting Eqs. (32) and (33) into Eq. (40), the following $2N + 1$ sets of linear equations with $2N + 2$ unknowns can be obtained:

$$\mathbf{C}\Delta\mathbf{A} = \mathbf{R} + \Delta\Omega\mathbf{R}_{mc} \tag{41}$$

where

$$C = \Omega_0^2 \mathbf{M} + \Omega_0 (\mathbf{C}_L + \mathbf{C}_{NL}) + (\mathbf{K}_L + \mathbf{K}_{NL}) \quad (42)$$

$$\mathbf{R} = - \left[\Omega_0^2 \mathbf{M} + \Omega_0 (\mathbf{C}_L + \mathbf{C}_{NL}) + \mathbf{K}_L \right] \mathbf{A}$$
$$- \mathbf{E}_N + \Omega_0^2 \mathbf{F} \quad (43)$$

$$\mathbf{R}_{mc} = - \left[2\Omega_0 \mathbf{M} + (\mathbf{C}_L + \mathbf{C}_{NL}) \right] \mathbf{A} + 2\Omega_0 \mathbf{F} \quad (44)$$

The unknown matrices derived in Eqs. (42)–(44) can be expressed as follows:

$$\mathbf{M} = \begin{bmatrix} \mu \mathbf{M}_1 & \mu \mathbf{M}_1 \\ \mathbf{M}_1 & \mathbf{0} \end{bmatrix}, \quad \mathbf{C}_L = \begin{bmatrix} \mathbf{0} & 2\xi c \mathbf{C}_1 \\ 2\xi \mathbf{C}_1 & -2\xi c \mathbf{C}_1 \end{bmatrix},$$

$$\mathbf{K}_L = \begin{bmatrix} \mathbf{0} & k\mathbf{K}_1 \\ \mathbf{K}_1 & -k\mathbf{K}_1 \end{bmatrix}, \mathbf{F} = \begin{bmatrix} \mu \mathbf{F}_1 \\ \mathbf{F}_1 \end{bmatrix},$$

$$\mathbf{C}_{NL} = \begin{bmatrix} \mathbf{0} & 2\xi c \mathbf{C}_2 \\ \mathbf{0} & -2\xi c \mathbf{C}_2 \end{bmatrix},$$

$$\mathbf{K}_{NL} = \begin{bmatrix} \mathbf{0} & k\mathbf{K}_2 \\ 2\alpha \mathbf{K}_3 & -k\mathbf{K}_2 \end{bmatrix}, \quad \mathbf{E}_N = \begin{bmatrix} k\mathbf{E}_1 \\ -k\mathbf{E}_1 + \alpha \mathbf{E}_2 \end{bmatrix}$$

where

$$\mathbf{M}_1 = \int_0^{2m\pi} \mathbf{C}_S^T \mathbf{C}_S'' d\tau, \quad \mathbf{C}_1 = \int_0^{2m\pi} \mathbf{C}_S^T \mathbf{C}_S' d\tau,$$

$$\mathbf{K}_1 = \int_0^{2m\pi} \mathbf{C}_S^T \mathbf{C}_S d\tau,$$

$$\mathbf{F}_1 = \int_0^{2m\pi} \mathbf{C}_S^T \sin(\tau) d\tau,$$

$$\mathbf{C}_2 = \int_0^{2m\pi} h_{(x_{20} - \Delta)} \mathbf{C}_S^T \mathbf{C}_S' d\tau,$$

$$\mathbf{K}_2 = \int_0^{2m\pi} h_{(x_{20} - \Delta)} \mathbf{C}_S^T \mathbf{C}_S d\tau,$$

$$\mathbf{K}_3 = \int_0^{2m\pi} x_{10} \mathbf{C}_S^T \mathbf{C}_S d\tau,$$

$$\mathbf{E}_1 = \int_0^{2m\pi} h_{(x_{20} - \Delta)} (x_{20} - \Delta) \mathbf{C}_S^T d\tau,$$

$$\mathbf{E}_2 = \int_0^{2m\pi} x_{10}^2 \mathbf{C}_S^T d\tau.$$

The elements of the above integration matrices can be referred to Appendix.

Because the number of unknowns is greater than the equations, one unknown should be set in advance as the control increment. To obtain the amplitude–frequency curves of the system by solving Eq. (41), many methods have been proposed [13,17–19] . The simplest way is to set $\Delta \Omega = 0$, and then, the Newton-Raphson interactions can be processed until the corrective vector norm $\|\mathbf{R}\|$ is smaller than a given convergence parameter.

However, the unstable solutions cannot be obtained by this method. For a more universal approach, the arc-length method is adopted to track the unstable equilibrium paths that involve the "snap-backs" phenomena. In this paper, Crisfield's procedure [29–31] is used to solve Eq. (41).

3.2 Stability of the periodic solution

Once the periodic solution is determined, the solution's stability can be investigated by the Floquet theory [17]. First, the small perturbation $\delta \mathbf{q}$ of $\mathbf{q}_0$ at Ω_0 can be expressed as

$$\mathbf{q} = \mathbf{q}_0 + \delta \mathbf{q} \quad (45)$$

By substituting Eq. (1) into Eq. (26), the linearized equation can be obtained for the small perturbation $\delta \mathbf{q}$ as follows:

$$\Omega_0^2 \bar{\mathbf{M}} \delta \ddot{\mathbf{q}} + \Omega_0 (\bar{\mathbf{C}}_L + \bar{\mathbf{C}}_{NL}) \delta \dot{\mathbf{q}} + (\bar{\mathbf{K}}_L + \bar{\mathbf{K}}_{NL}) \delta \mathbf{q} = 0 \quad (46)$$

Transforming above equations into linear ordinary differential equations,

$$\dot{\mathbf{Z}} = \mathbf{Q}(\tau) \mathbf{Z} \quad (47)$$

where

$$\mathbf{Z} = \begin{bmatrix} \delta q_1, \delta q_2 \end{bmatrix}^T, \mathbf{Q}(\tau)$$
$$= \begin{bmatrix} \mathbf{0} & \mathbf{I} \\ -\dfrac{\bar{\mathbf{K}}_L + \bar{\mathbf{K}}_{NL}}{\Omega_0^2 \bar{\mathbf{M}}} & -\dfrac{\bar{\mathbf{C}}_L + \bar{\mathbf{C}}_{NL}}{\Omega_0 \bar{\mathbf{M}}} \end{bmatrix} \quad (48)$$

$\mathbf{0}$ is the 2×2 null matrix, and $\mathbf{I}$ is the 2×2 unit matrix. It can be seen that matrix $\mathbf{Q}(\tau)$ has the same period with $\mathbf{q}_0$ [15]. Friedmann [32] proposed an efficient numerical approach to approximate the periodic matrix with a set of step functions, namely the matrix $\mathbf{Q}(\tau)$ keeps the same figure in a relatively small range of time. In this case, period $2m\pi$ is divided into N_k intervals for numerical computation, and the kth interval is $[\tau_{k-1}, \tau_k]$ with the interval length of $\Delta_k = \tau_k - \tau_{k-1}$. Thus, the constant matrix $\mathbf{C}_k$ can be written as

$$\mathbf{C}_k = \frac{1}{\Delta_k} \int_{\tau_{k-1}}^{\tau_k} \mathbf{Q}(\tau) d\tau \quad (49)$$

After the constant matrix $\mathbf{C}_k$ is obtained, the transition matrix or the monodromy matrix, which is used to decide the stability of the system, can be expressed:

$$\mathbf{P} = \prod_{i=1}^{N_k} \exp(\mathbf{C}_k \Delta_k) \qquad (50)$$

The terms $\exp(\mathbf{C}_k \Delta_k)$ are expanded with the Taylor formula for programming:

$$\mathbf{P} = \prod_{i=1}^{N_k} \left(\mathbf{I} + \sum_{j=1}^{M} \frac{[\Delta_i \mathbf{C}_i]^j}{j!} \right) \qquad (51)$$

where M is the number of terms in the approximation of the constant matrix exponential [18]. In this paper, M is set to 4. The stability of the solution can be decided by the eigenvalues of matrix $\mathbf{P}$ which are called Floquet multipliers [17]. If any of the Floquet multipliers has a module that is greater than one, then the solution is unstable. Namely [15],

(1) A real Floquet multiplier moves out of the unit circle, and the remaining Floquet multipliers stay inside the unit circle; and

(2) A pair of conjugate Floquet multipliers move out of the unit circle, and the remaining Floquet multipliers stay inside the unit circle.

For sub-harmonic resonances, a proper value of m can be set to acquire the $1/m$ sub-harmonic resonance of the system, and the stability of these responses can also be checked by the above procedure.

4 Numerical simulation and discussion

4.1 Numerical simulation and validation

To demonstrate the accuracy of IHBM, the amplitude–frequency curves and phase diagrams of the piecewise-

Table 1 System parameters

Parameter	Description/units	Value
m_1	Unsprung mass (kg)	472.5
k_1/k_1^*	Stiffness of the tire (N/mm/ N/mm^2)	560.0 /1.2
c_1	Damping of the tire (Ns/mm)	2.10
k_2/k_3	Stiffness of the suspension (N/mm)	159.87 /206.23
c_2/c_3	Damping of the suspension (Ns/mm)	1.392/1.580
e	Original distance between springs (mm)	60
r	Amplitude of the road profile (mm)	10

Table 2 Computation results of IHBM on different values of N_m for $\mu_{cr} = 2.0698$ and $\Omega = 0.36$

Number of the harmonic terms, N_m	Amplitude of the displacements		Amplitude of the velocities	
	x_1	x_2	x_1	x_2
1	3.7417	7.7137	3.7417	7.7137
2	3.9345	8.0130	4.9810	8.4133
3	4.0653	7.6549	5.0153	9.0176
6	4.0033	7.4661	4.8157	8.8966
12	3.9983	7.4630	4.8169	8.9293
RKM	3.9946	7.4595	4.8114	8.9346

linear quarter-car model are solved by both IHBM and the Runge–Kutta method (RKM). System parameters used in the simulation are given in Table 1.

Here, the simulations are presented with the sprung mass ratio of $\mu_{cr} = 2.0698 (m_2 = m_{2cr})$. First, the number of the harmonic terms N_m in the simulation is investigated. It can be seen from the Table 2 that the results of IHBM are close to the solution presented by RKM with increasing value of N_m. When $N_m = 1$, the solution obtained with IHBM, which can be regarded as the solution obtained with the average method, does not match well with the result of RKM. To improve the accuracy of simulation and to save the computation consumption, N_m is set to 6 in this paper.

Then, Figs. 3 and 4 show the nonlinear dynamic responses of the quarter-car model by using both IHBM and RKM, and the results are in good agreement with one another. Figure 3 shows the phase diagrams of both DOFs at the non-dimensional frequencies $\Omega = 0.36$ and $\Omega = 1.20$, which indicate the two peaks of the frequency response curves. In Fig. 3, the solid line '-' denotes the IHBM solutions, and the dot denotes the RKM solutions. In the primary resonance peak, more than one harmonic term contributes to the vibration of both DOFs under one external harmonic excitation, which shows nonlinear characteristics of the system. However, in the second resonance peak, only one harmonic term works which indicates that the nonlinearity is weak at the presented state.

An interesting phenomenon can be found when the sprung mass ratio is close to a certain value. In Fig. 4, the frequency response curves of both DOFs with a mass ratio of $\mu_{cr} = 2.0698$ are studied. The black circle represents the numerical results from RKM, and
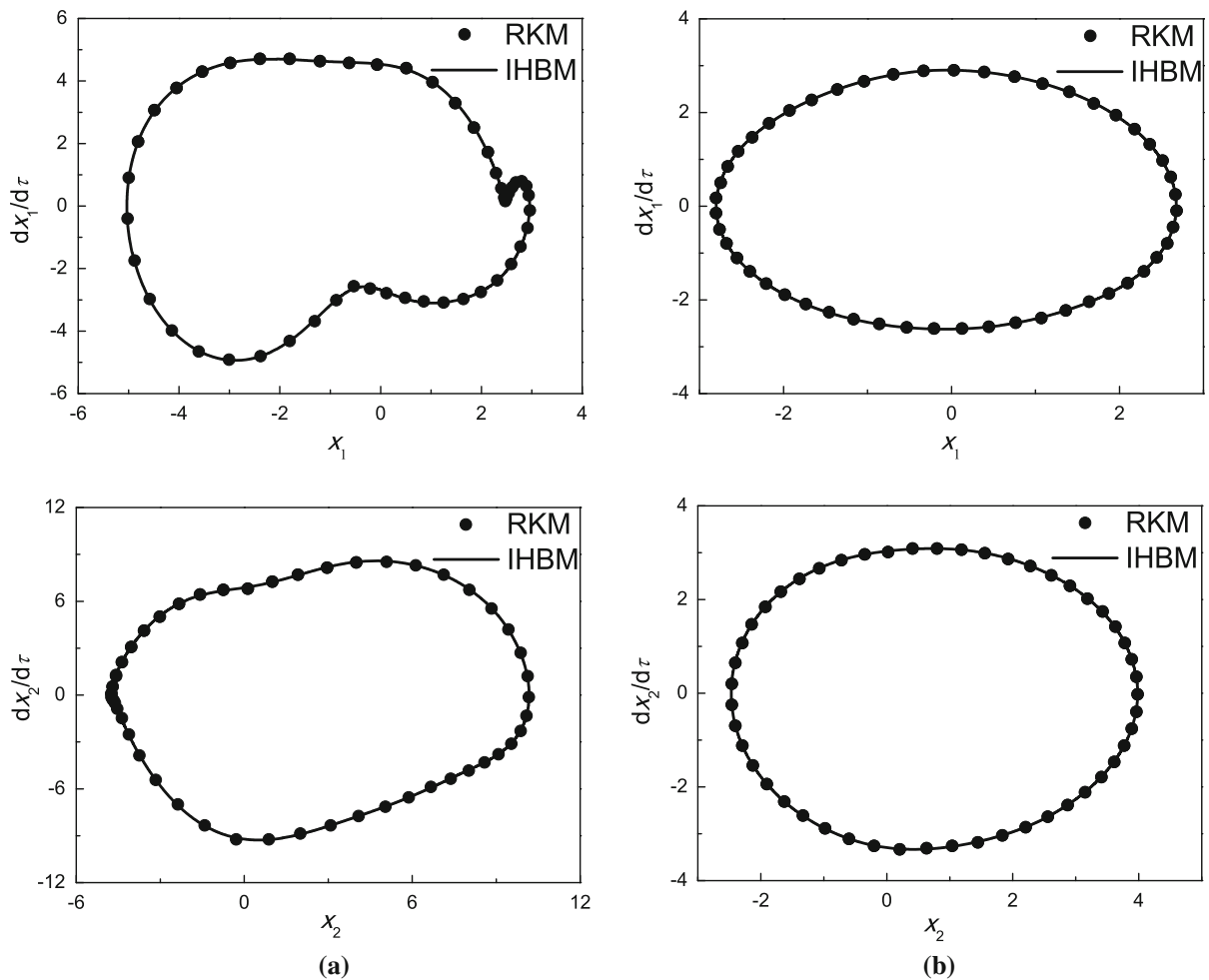
Fig. 3 Phase diagrams of the system DOFs at **a** $\Omega = 0.4$ and **b** $\Omega = 1.2$

the solid line denotes the calculation solutions from IHBM. It can be observed from Fig. 4c that between $\Omega = 0.6803$ and $\Omega = 0.7457$, the fundamental solutions lose stabilities with one of their Floquet multipliers that leaves the unit circle. This finding is consistent with Fig. 4a, b, and the period-1 solutions of IHBM do not match with the period-1 solutions of RKM in this unstable region, which means that sub-harmonic or chaos resonances exist in this region. Figure 5 shows 1/2 sub-harmonic response of both DOFs at $\Omega = 0.70$, and it can be seen that the harmonic terms 0.5Ω and 1.5Ω play an important role in vibration responses. In Fig. 6, the sub-harmonic resonances of these unstable regions are investigated. The black solid and dashed lines denote the stable and unstable solutions, respectively, of the fundamental reso-

nances with IHBM, and the red solid line represents the sub-harmonic resonances with IHBM. The 1/2 sub-harmonic resonances can be found with the "snapback" phenomenon, which indicates the strong coupled nonlinearities of both DOFs in this region. This finding is different from the SDOF piecewise-linear system. Other $1/m$ sub-harmonic resonances are not found in the frequency response curves, mainly because of the existence of the second order resonance of the system.

4.2 Effect of the auxiliary leaf spring's stiffness on the dynamic response of the system

The auxiliary leaf spring's stiffness that is discussed in this section is an essential parameter for suspension
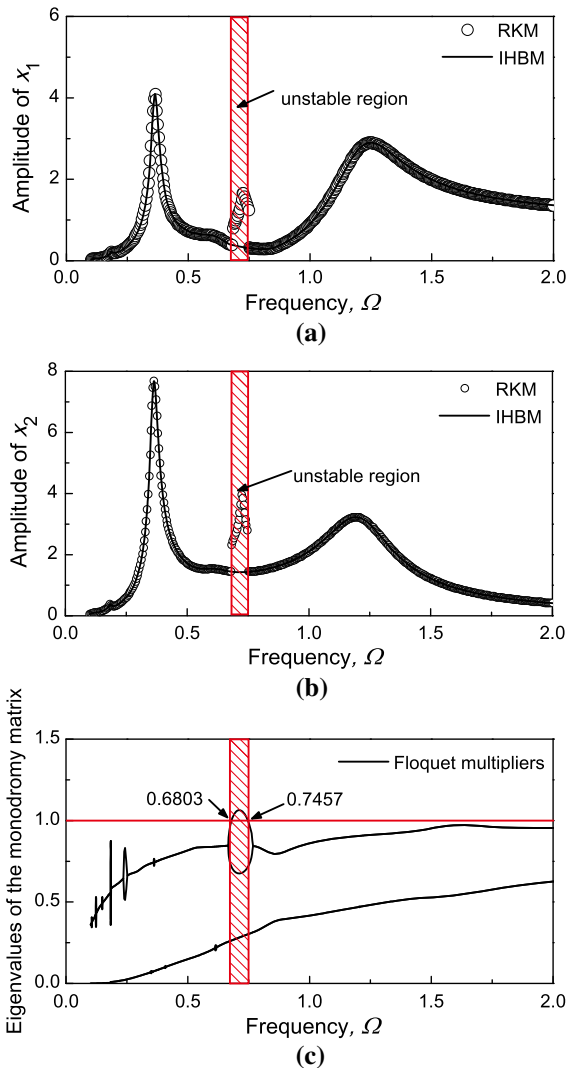
Fig. 4 Response diagram for $\mu = 2.0698$: **a** frequency response curve of the amplitude of x_1, **b** frequency response curve of the amplitude of x_2 and **c** the eigenvalues of the monodromy matrix compared with Ω

design. As seen in Fig. 4, two resonance peaks exist in the frequency response curves, and the primary resonance peak that represents the resonance of x_2 has a larger amplitude. To reduce the vibrations of the model, the effect of the auxiliary leaf spring's stiffness ratio ν_3 on the primary resonance peak is discussed in this section. The frequency response curves of the x_2 of different load states with five different auxiliary leaf spring stiffness ratios, namely $\nu_3 = 0.184, 0.285, 0.368, 0.736$ and 1.104, are shown in Figs. 7 and 8. The black solid line denotes the system in which the

stiffnesses of the main and auxiliary leaf spring are the same, and the black dash dot line represents the absolute value of the critical distance of each case.

Usually, the stiffness of the auxiliary leaf spring is set a larger value than that of the main leaf spring. It can be seen from these figures that the existence of the auxiliary leaf spring with larger stiffness will decrease the maximum amplitude in both the light and heavy load states. Thus, a proper design of the auxiliary leaf spring can contribute to the reduction in the suspension vibration. In addition, at the light load state, when the displacement of x_2 increases, the spring of suspension becomes stiff as the stiffness changes from k_2 to $k_2 + k_3$. As a result, the system shows a "harden" characteristic, which is similar to a "harden" Duffing oscillator [33]. It can be seen from Fig. 7 that the resonance peak of the frequency response curve moves to the right when the displacement of x_2 is greater than the absolute value of Δ_1. The similarity of the heavy load state system to the "soft" Duffing oscillator can also be concluded.

4.3 Effect of the sprung mass ratio on the dynamic response of the system

In this section, the effect of the sprung mass ratio μ on the dynamic responses of the piecewise quarter-car model is investigated with IHBM, and the other parameters remain the same as in previous analyses. From Fig. 9, when the sprung mass ratio μ is larger, the amplitude of both x_1 and x_2 are larger for the primary resonance. It can be concluded that if the truck is overloaded, it will be very dangerous because the amplitude of the displacement can exceed the designed dynamic deflection of the suspension.

In addition, the sub-harmonic resonances can be found on some sprung mass ratios that are close to a certain value. The existence of an unstable region where the frequency varies from 0.6 to 0.9 can be determined by the Floquet multipliers for all of the possible sprung mass ratios of μ from 1.25 to 3.0. This unstable region that includes $1/m$ sub-harmonic resonances or chaotic vibration will greatly increase the response amplitude in this frequency region, which is shown in Fig. 9.

From Fig. 10, the unstable region occurs when the sprung mass ratio μ changes from 1.508 to 2.767. The entire unstable region that comprises the frequency and the mass ratio presents a 'gourd' shape, and the bound-
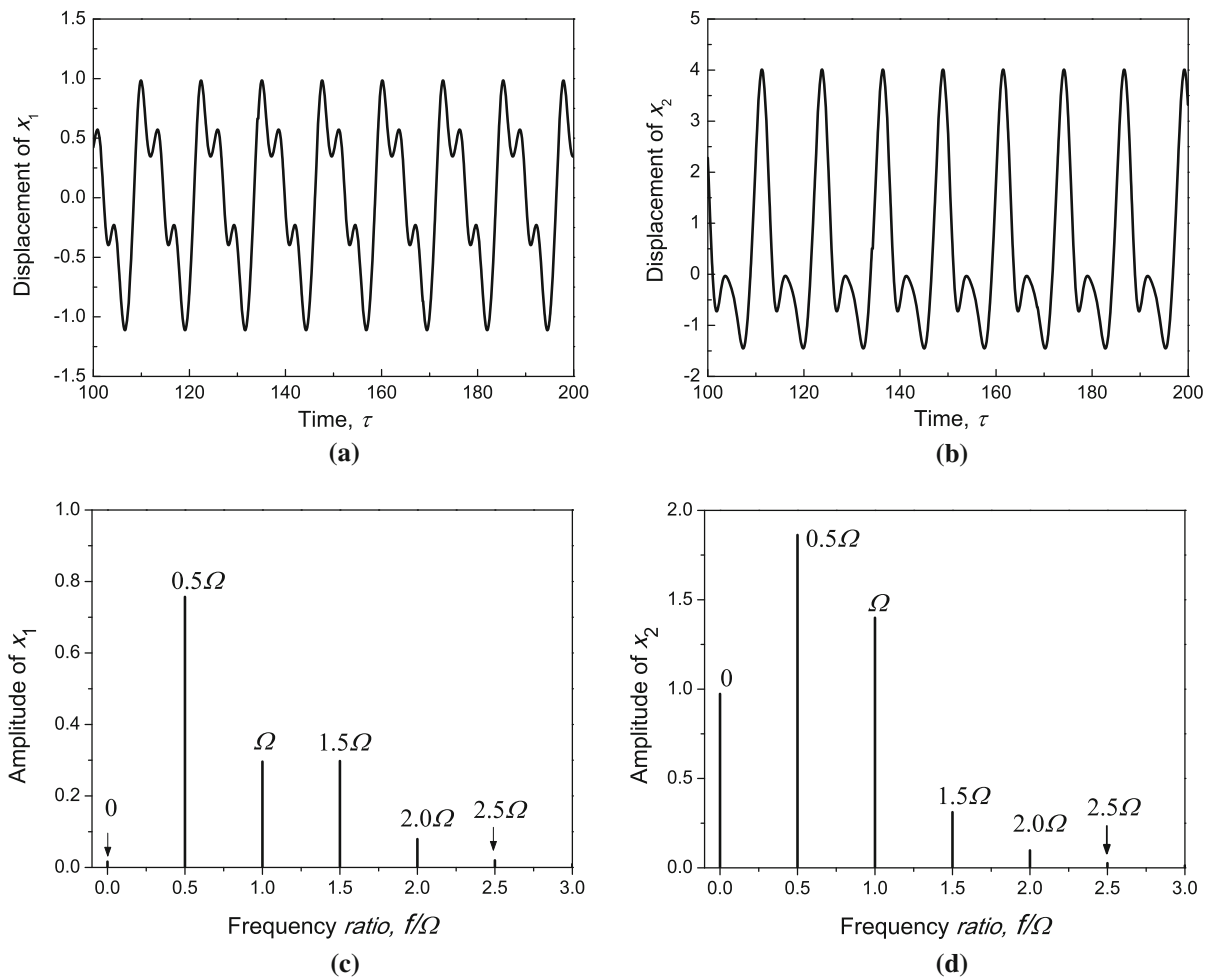
Fig. 5 Vibration of 1/2 sub-harmonic response for $\Omega = 0.7$: **a** time history of x_1, **b** time history of x_2, **c** Fourier spectrum of x_1 and **d** Fourier spectrum of x_2

ary frequencies of the unstable region decrease with the mass ratio increases until $\mu \approx 2.40$ where the maximum difference between the upper and lower boundary frequencies occurs. Afterward, the difference begins to decrease and become zero when $\mu = 2.767$.

4.4 Effect of the main leaf spring's damping on the dynamic response of the system

In Sect. 4.3 the unstable region is discussed for various sprung mass ratios, and these regions should be avoided in engineering by changing the system parameters. The proper way to avoid these regions is to add a vibration isolation system to increase the main leaf spring's damping of the suspension [19,25].

In this section, the effect of the main leaf spring's damping on the dynamic response of system is discussed, and other parameters remain the same. Figure 11 shows that with the increasing damping coefficient of the main leaf spring, the fundamental tendency of the frequency response curves remains unchanged, but the amplitudes of the primary resonance and the sub-harmonic resonance decrease markedly for both DOFs. Meanwhile, the frequency interval of the unstable region will be reduced with greater values of damping coefficients, and when the damping coefficients $\eta_2 = 1.6000\,(\mu = \mu_{cr})$, an unstable region is not detected.

Based on the above analysis, the main leaf spring's damping will decrease the sub-harmonic resonance, Fig. 12 illustrates the unstable region that is calculated for different main leaf springs' damping coefficients
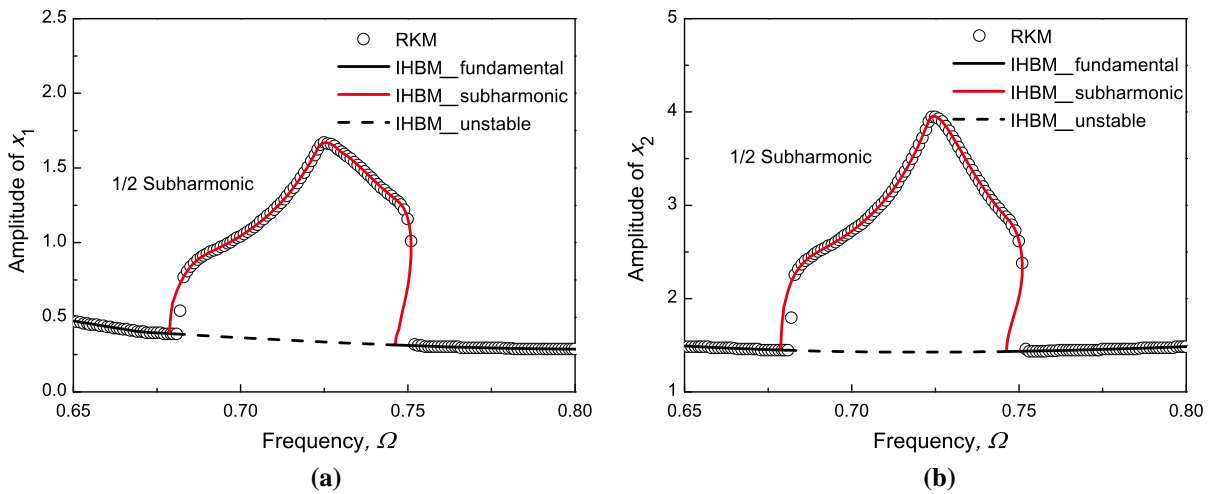
Fig. 6 Partial enlarged plot of the unstable region of $\mu_{cr} = 2.0698$: **a** frequency response curve of the amplitude of x_1 and **b** Frequency response curve of the amplitude of x_2
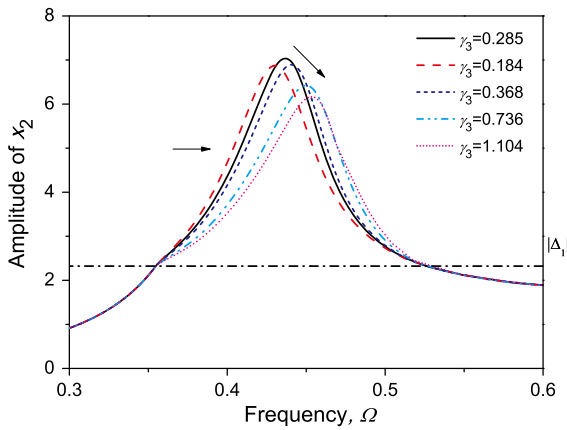

Fig. 7 Partial enlarged plot of the frequency response curves of the amplitude of x_2 in the light load state case where $\mu = 1.2698$
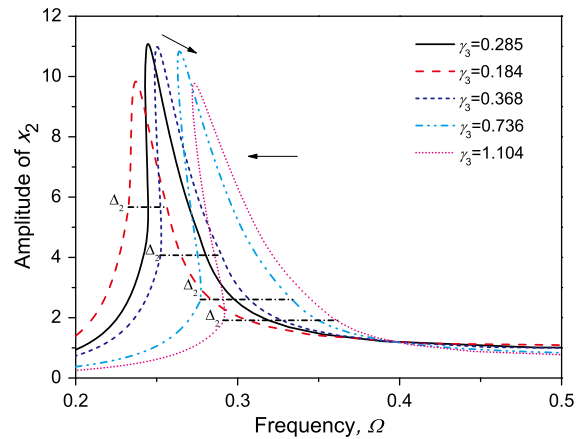

Fig. 8 Partial enlarged plot of the frequency response curves of the amplitude of x_2 in the heavy load state case where $\mu = 5.2910$

for all of the possible sprung masses of m_2 from 600 to 1400 kg ($\eta_2 = 0.3310$, $\eta_2 = 0.6628$, $\eta_2 = 0.9930$, and $\eta_2 = 1.6000$). According to Fig. 12, when the value of η_2 grows, the unstable region quickly diminishes. For $\eta_2 \approx 1.617$, all of the Floquet multipliers are in the unit circle, which indicates that all of these solutions are stable. This results can be instructive for the design of a suspension vibration absorber.

5 Conclusion

In this study, the nonlinear dynamic behavior of a 2-DOF quarter-car truck model with a piecewise-linear leaf spring is studied with IHBM. The effect of the auxiliary leaf spring's stiffness, the sprung mass ratio and the main leaf spring's damping on the nonlinear dynamic responses are discussed. The results can be summarized as follows.

1. The periodic motion of the system is investigated with IHBM, and the results obtained by IHBM compare well with the results that are calculated by the RKM. The sub-harmonic resonance on the frequency response curve can be found with the 'snap-back' characteristic due to the coupled influence of both DOFs.

2. The effect of the auxiliary leaf spring's stiffness on the dynamic response of the system is investi-
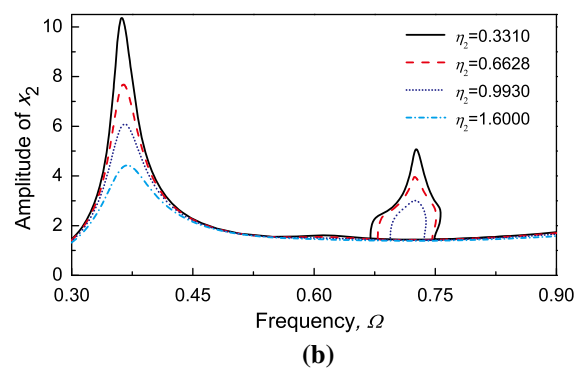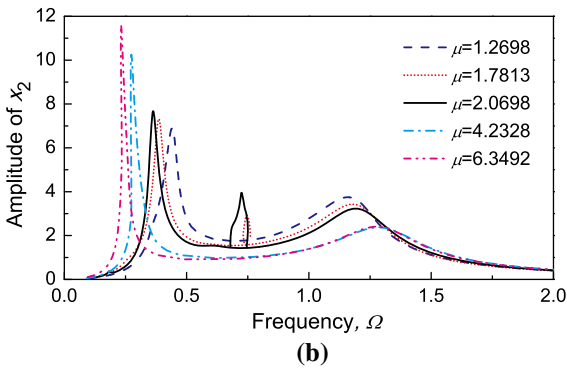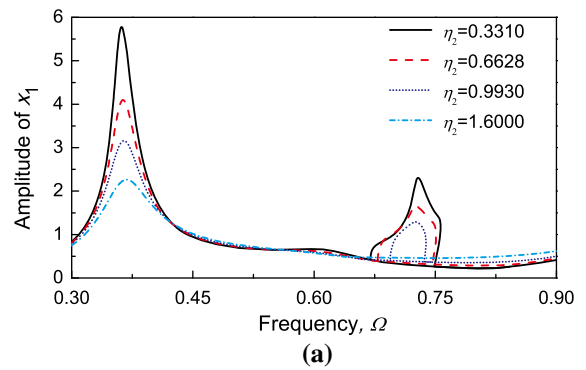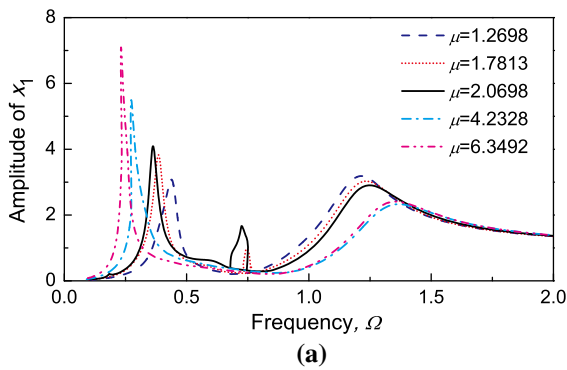
Fig. 9 Frequency response curves for different unsprung mass ratios: **a** frequency response curve of the amplitude of x_1 and **b** frequency response curve of the amplitude of x_2

Fig. 11 Frequency response curves for $\mu = 2.0698$: **a** frequency response curve of the amplitude of x_1 and **b** frequency response curve of the amplitude of x_2
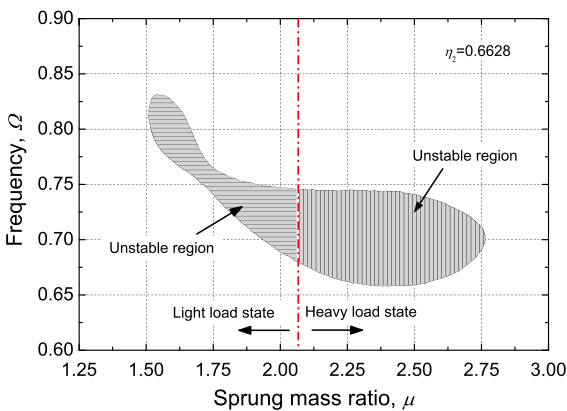

Fig. 10 Unstable region calculated by the Floquet theory for mass ratio from 1.25 to 3.0 and frequencies from 0.6 to 0.9 (the shadow region refers to the unstable region)
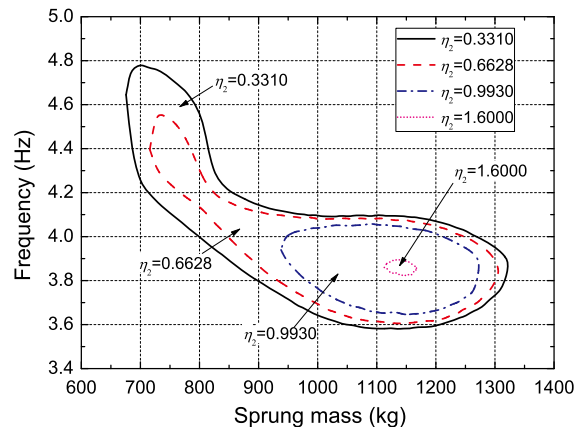

Fig. 12 Unstable region calculated by the Floquet theory for different main leaf springs' damping coefficients

gated. The piecewise-linear stiffness of a leaf spring shares similar characteristics with the stiffness of a Duffing oscillator. Additionally, the proper design of an auxiliary leaf spring contributes to the reduction in the suspension vibration.

3. The effect of the sprung mass ratio on the dynamic response of the system is investigated. The amplitudes of both x_1 and x_2 for the primary resonance are found to increase as the sprung mass increase.

The unstable region will occur at certain sprung mass ratios.

4. The effect of the main leaf spring's damping on the dynamic response of the system is investigated. It is found that when the damping coefficient increases, the amplitude of the response curve, as well as the unstable region, has a significance decline. When $\eta_2 \approx 1.617$, the unstable region is diminished.

Appendix

The analytical expressions of the unknown matrices are listed below:

$$[\mathbf{M}_1]_{ij} = \begin{cases} \frac{j^2\pi\delta_{ij}}{m}, & i = 0, 1, \ldots, N; j = 0, 1, \ldots, N \\ \frac{(j-N)^2\pi\delta_{ij}}{m}, & i = N+1, \ldots, 2N; \\ & j = N+1, \ldots, 2N \end{cases}$$

$$[\mathbf{C}_1]_{ij} = \begin{cases} j\pi\beta_{ij}, & i = 0, 1, \ldots, N; j = 0, 1, \ldots, N \\ (j-N)\pi\beta_{ij}, & i = N+1, \ldots, 2N; \\ & j = N+1, \ldots, 2N \end{cases}$$

$$[\mathbf{K}_1]_{ij} = \alpha_i m\pi\delta_{ij}, i = 0, 1, \ldots, N; j = 0, 1, \ldots, N$$

$$\mathbf{C}_2 = \begin{bmatrix} \mathbf{C}_2^{cc} & \mathbf{C}_2^{cs} \\ \mathbf{C}_2^{sc} & \mathbf{C}_2^{ss} \end{bmatrix}, \mathbf{K}_2 = \begin{bmatrix} \mathbf{K}_2^{cc} & \mathbf{K}_2^{cs} \\ \mathbf{K}_2^{sc} & K_2^{ss} \end{bmatrix}, \mathbf{E}_1 = \begin{bmatrix} \mathbf{E}_1^c \\ \mathbf{E}_1^s \end{bmatrix}$$

Consider a period 2π, where $\theta_0 = 0$ and $\theta_{M+1} = 2\pi$. There are M zeros of $q_{20} = \Delta$, denote as $\theta_1, \theta_2, \ldots \theta_M$ ($\theta_1 < \theta_2 < \ldots < \theta_M$).

$$[\mathbf{C}_2^{cc}]_{ij} = -\alpha_i j \sum_{l=0}^{M} h_{(q_{20}-\Delta)}(B_{ij}(\theta_{l+1}) - B_{ij}(\theta_l)), i = 0, 1, \ldots, N; j = 0, 1, \ldots, N$$

$$[\mathbf{C}_2^{cs}]_{ij} = \alpha_i j \sum_{l=0}^{M} h_{(q_{20}-\Delta)}(A_{ij}(\theta_{l+1}) - A_{ij}(\theta_l)), i = 0, 1, \ldots, N; j = 1, \ldots, N$$

$$[\mathbf{C}_2^{sc}]_{ij} = -j \sum_{l=0}^{M} h_{(q_{20}-\Delta)}(D_{ij}(\theta_{l+1}) - D_{ij}(\theta_l)), i = 1, \ldots, N; j = 0, 1, \ldots, N$$

$$[\mathbf{C}_2^{ss}]_{ij} = j \sum_{l=0}^{M} h_{(q_{20}-\Delta)}(C_{ij}(\theta_{l+1}) - C_{ij}(\theta_l)), i = 1, \ldots, N; j = 1, \ldots, N$$

$$[\mathbf{K}_2^{cc}]_{ij} = \alpha_i\alpha_j m \sum_{l=0}^{M} h_{(q_{20}-\Delta)}(A_{ij}(\theta_{l+1}) - A_{ij}(\theta_l)), i = 0, 1, \ldots, N; j = 0, 1, \ldots, N$$

$$[\mathbf{K}_2^{cs}]_{ij} = \alpha_i m \sum_{l=0}^{M} h_{(q_{20}-\Delta)}(B_{ij}(\theta_{l+1}) - B_{ij}(\theta_l)), i = 0, 1, \ldots, N; j = 1, \ldots, N$$

$$[\mathbf{K}_2^{sc}]_{ij} = \alpha_j m \sum_{l=0}^{M} h_{(q_{20}-\Delta)}(C_{ij}(\theta_{l+1}) - C_{ij}(\theta_l)), i = 1, \ldots, N; j = 0, 1, \ldots, N$$

$$[\mathbf{K}_2^{ss}]_{ij} = m \sum_{l=0}^{M} h_{(q_{20}-\Delta)}(D_{ij}(\theta_{l+1}) - D_{ij}(\theta_l)), i = 1, \ldots, N; j = 1, \ldots, N$$

$$[\mathbf{E}_1^c]_i = m \sum_{l=0}^{M} h_{(q_{20}-\Delta)} \left\{ \sum_{j=0}^{N} \alpha_j \left[a_{1j}(A_{ij}(\theta_{l+1}) - A_{ij}(\theta_l)) + b_{1j}(B_{ij}(\theta_{l+1}) - B_{ij}(\theta_l)) \right] - \Delta(E_{ij}(\theta_{l+1}) - E_{ij}(\theta_l)) \right\}, i = 0, \ldots, N$$

$$[\mathbf{E}_1^s]_i = m \sum_{l=0}^{M} h_{(q_{20}-\Delta)} \left\{ \sum_{j=0}^{N} \alpha_j \left[a_{1j}(C_{ij}(\theta_{l+1}) - C_{ij}(\theta_l)) + b_{1j}(D_{ij}(\theta_{l+1}) - D_{ij}(\theta_l)) \right] - \Delta(F_{ij}(\theta_{l+1}) - F_{ij}(\theta_l)) \right\}, i = 1, \ldots, N$$

$$[\mathbf{K}_3]_{i,j} = \frac{m\pi}{4} \begin{cases} a_{10}, & i = 0; j = 0 \\ 2a_{1i}, & i \neq 0; j = 0 \\ 2a_{1j}, & i = 0; j \neq 0 \\ 2(a_{1(i+j)} + \varphi_{ij}a_{1|i-j|}), & \text{otherwise} \end{cases}$$

$$q_{20}^2 = \left[\frac{1}{2}a_{20} + \sum_{i=1}^{N} \left(a_{2i}\cos\frac{i\pi}{m} + b_{2i}\sin\frac{i\pi}{m} \right) \right]^2$$

$$= G_0 + \sum_{i=1}^{2N} \left(G_i \cos\frac{i\pi}{m} + H_i \sin\frac{i\pi}{m} \right)$$

$$[\mathbf{E}_2]_i = m\pi \begin{cases} G_0, & i = 0 \\ G_i, & i = 1, \ldots, N \\ H_{i-N}, & i = N+1, \ldots, 2N \end{cases}$$

where $\delta_{ij} = \begin{cases} 1, & i = j \\ 0, & i \neq j \end{cases}$, $\alpha_i = \begin{cases} 0.5, & i = 0 \\ 1, & i \neq 0 \end{cases}$, $\beta_{ij} = \begin{cases} -1, & i = j + N \\ 1, & j = i + N \\ 0, & \text{otherwise} \end{cases}$, $\varphi_{ij} = \begin{cases} 2, & i = j \\ 1, & i \neq j \end{cases}$. And expressions of $A_{ij}, B_{ij}, C_{ij}, D_{ij}, E_i, F_i$ can be referred to Wong [18].

References

1. Jazar, R.N.: Vehicle Dynamics: Theory and Application. Springer, New York (2008)
2. Zhou, S., Song, G., Sun, M., et al.: Nonlinear dynamic analysis of a quarter vehicle system with external periodic excitation. Int. J. Nonlinear Mech. **84**, 82–93 (2016)
3. Litak, G., Borowiec, M., Ali, M., et al.: Pulsive feedback control of a quarter car model forced by a road profile. Chaos Soliton Fract. **33**(5), 1672–1676 (2006)
4. Litak, G., Borowiec, M., Friswell, M.I., et al.: Chaotic vibration of a quarter-car model excited by the road surface profile. Commun. Nonlinear Sci. **13**(7), 1373–1383 (2006)
5. Türkay, S., Akçay, H.: A study of random vibration characteristics of the quarter-car model. J. Sound Vib. **282**(1–2), 111–124 (2005)
6. Li, S., Yang, S., Guo, W.: Investigation on chaotic motion in hysteretic non-linear suspension system with multi-frequency excitations. Mech. Res. Commun. **31**(2), 229–236 (2004)
7. Borowiec, M., Litak, G.: Transition to chaos and escape phenomenon in two-degrees-of-freedom oscillator with a kinematic excitation. Nonlinear Dyn. **70**(2), 1125–1133 (2012)
8. Zhong, S., Chen, Y.: Bifurcation of piecewise-linear nonlinear vibration system of vehicle suspension. Appl. Math. Mech. Eng. **30**(6), 677–684 (2009)
9. Li, Y.H., Chen, S.D.: Bifurcation induced by mass variation in piecewise linear system. Appl. Mech. Mater. **226–228**, 531–535 (2012)
10. Silveira, M., Wahi, P., Fernandes, J.C.M.: Effects of asymmetrical damping on a 2 DOF quarter-car model under harmonic excitation. Commun. Nonlinear Sci. **43**, 14–24 (2017)
11. Deshpande, S., Mehta, S., Jazar, G.N.: Optimization of secondary suspension of piecewise linear vibration isolation systems. Int. J. Mech. Sci. **48**(4), 341–377 (2006)
12. Bajkowski, J., Szemplinska-Stupnicka, W.: Internal resonances effects-simulation versus analytical methods results. J. Sound Vib. **104**, 259–275 (1986)
13. Cheung, Y.K., Chen, S.H., Lau, S.L.: Application of the incremental harmonic balance method to cubic non-linearity systems. J. Sound Vib. **140**(2), 273–286 (1990)
14. Shen, Y.J., Wen, S.F., Li, X.H., et al.: Dynamical analysis of fractional-order nonlinear oscillator by incremental harmonic balance method. Nonlinear Dyn. **85**(3), 1457–1467 (2016)
15. Shen, J.H., Lin, K.C., et al.: Bifurcation and route-to-chaos analyses for Mathieu-Duffing oscillator by the incremental harmonic balance method. Nonlinear Dyn. **52**(4), 403–414 (2008)
16. Wang, X.F., Zhu, W.D.: A modified incremental harmonic balance method based on the fast Fourier transform and Broyden's method. Nonlinear Dyn. **81**(1–2), 1–9 (2015)
17. Yuanping, L., Siyu, C.: Periodic solution and bifurcation of a suspension vibration system by incremental harmonic balance and continuation method. Nonlinear Dyn. **83**(1–2), 941–950(2016)
18. Wong, C.W., Zhang, W.S., Lau, S.L.: Periodic forced vibration of unsymmetrical piecewise-linear systems by incremental harmonic balance method. J. Sound Vib. **149**(1), 91–105 (1991)
19. Lau, S.L., Zhang, W.S.: Nonlinear vibrations of piecewise-linear systems by incremental harmonic balance method. J. Appl. Mech. **59**(1), 153–160 (1992)
20. Raghothama, A., Narayanan, S.: Bifurcation and chaos in escape equation model by incremental harmonic balancing. Chaos Soliton Fract. **11**(9), 1349–1363 (2000)
21. Raghothama, A., Narayanan, S.: Bifurcation and chaos of an articulated loading platform with piecewise non-linear stiffness using the incremental harmonic balance method. Ocean Eng. **27**(10), 1087–1107 (2000)
22. Xu, L., Lu, M.W., Cao, Q.: Nonlinear vibrations of dynamical systems with a general form of piecewise-linear viscous damping by incremental harmonic balance method. Phys. Lett. A **301**(1–2), 65–73 (2002)
23. Xu, L., Lu, M.W., Cao, Q.: Bifurcation and chaos of a harmonically excited oscillator with both stiffness and viscous damping piecewise linearities by incremental harmonic balance method. J. Sound Vib. **264**(4), 873–882 (2003)
24. Kim, T.C., Rook, T.E., Singh, R.: Super- and sub-harmonic response calculations for a torsional system with clearance nonlinearity using the harmonic balance method. J. Sound Vib. **281**(3–5), 965–993 (2005)
25. Duan, C., Singh, R.: Isolated sub-harmonic resonance branch in the frequency response of an oscillator with slight asymmetry in the clearance. J. Sound Vib. **314**(1–2), 12–18 (2008)
26. Ma, Q., Kahraman, A.: Subharmonic resonance of a mechanical oscillator with periodically time-varying, piecewise-nonlinear stiffness. J. Sound Vib. **294**(3), 624–636 (2006)
27. Kong, X., Sun, W., Wang, B., et al.: Dynamic and stability analysis of the linear guide with time-varying, piecewise-nonlinear stiffness by multi-term incremental harmonic balance method. J. Sound Vib. **346**(1), 265–283 (2015)
28. Xiong, H., Kong, X., Li, H., et al.: Vibration analysis of nonlinear systems with the bilinear hysteretic oscillator by using incremental harmonic balance method. Commun. Nonlinear Sci. **42**, 437–450 (2017)
29. Crisfield, M.A.: A fast incremental/iterative solution procedure that handles "snap-through". Comput. Struct. **13**(1), 55–62 (1981)
30. Fafard, M., Massicotte, B.: Geometrical interpretation of the arc-length method. Comput. Struct. **46**(4), 60–65 (1993)
31. Feng, Y.T., Peric, D., Owen, D.R.J.: Determination of travel directions in path-following methods. Math. Comput. Model. **21**(7), 43–59 (1995)
32. Friedmann, P., Hammond, C.E., Woo, T.H.: Efficient numerical treatment of periodic systems with application to stability problems. Int. J. Numer. Meth. Eng. **11**(7), 1117–1136 (1976)
33. Kovacic, I., Brennan, M.J.: The Duffing Equation: Nonlinear Oscillators and Their Behaviour. Wiley, Chichester (2011)